

## Analysis of Nitrogen Ion Implantation on Corrosion Inhabitation of Zirconium Nitride Coated 304 Stainless Steel and Correlation with Nano-structure and Surface Hardness

M. Karimi, A. R. Grayeli\*

Physics and Accelerators Research School, Nuclear Science & Technology Research Institute, P.O. Box: 11365-3486, Tehran, Iran.

### ARTICLE INFO

Article history:

Received: 11 Apr 2023

Final Revised: 06 July 2023

Accepted: 08 July 2023

Available online: 17 Sep 2023

Keywords:

Zirconium thin film

Ion implantation

Corrosion

Hardness

Stainless steel

### ABSTRACT

One of the common methods to improve and change the structural, wear, and corrosion characteristics of materials is to create a resistant thin film using the physical vapor deposition process. Various ions are substituted or interspersed on the surface of metal or non-metal parts using accelerators. This article investigates the structural, corrosion, and mechanical properties (hardness) of zirconium nitride coatings prepared by ion beam sputtering and nitrogen ion implantation on 304 stainless steel. For this purpose, a coating of zirconium with a thickness of 100 nm has been deposited on 304 stainless steel by the ion beam sputtering method. Nitrogen ion implantation was performed at a temperature of 400 K and a dose of  $5 \times 10^{17} \text{ N}^+ \text{ cm}^{-2}$  at energies of 10, 20, 40, and 80 keV. The crystallographic investigation, hardness, corrosion tests in 0.6 M NaCl solution, and SEM were done for different samples. The correlation between the test results, considering the increase in the implantation energy, introduced the optimal energy of 40 keV to make the sample with the highest degree of corrosion resistance and hardness. Prog. Color Colorants Coat. 16 (2023), 409-415 © Institute for Color Science and Technology.

### 1. Introduction

The use of thin films for protection has been of interest to humans for a long time. Many modern and complex electronic and optical parts are made in thin film [1-4]. Over the past few years, transition metal nitrides have emerged as the most promising coating options for enhancing the corrosion resistance of less noble materials like steel. Despite possessing beneficial properties such as chemical stability, hardness, good adhesion to steel substrates, and attractive colors, metal nitrides coatings tend to exhibit poor corrosion resistance due to the presence of certain imperfections, including pores, cracks, pinholes, and transient grain boundaries. Physical vapor deposition techniques, in particular, often

result in a high density of microscopic defects within the coating structure, making the film vulnerable to corrosion attack. Essentially, the presence of these defects creates paths that allow corrosive media to penetrate the substrate, compromising the system's corrosion resistance. Consequently, researchers have explored various techniques to improve the coatings' quality [5-8].

Recently, compared to other metal nitrides, zirconium nitride thin film has been used the most in industrial fields, such as hard coatings, corrosion-resistant coatings, and creating penetration barriers in microelectronic devices. The formation of zirconium nitride coatings is more complex than TiN or CrN films

\*Corresponding author: \* a\_grayli@yahoo.com

Doi: 10.30509/pccc.2023.167128.1213

because zirconium has a high melting point and low vapor pressure and is highly susceptible to oxygen and carbon pollution. Fewer studies have been done about zirconium nitride compared with nitride films of other transition metals [9-11].

To deposit zirconium nitride on different substrates, a long time and high temperature are required; therefore, various methods of physical vapor deposition (PVD) have been used to increase the deposition rate and lower the temperature [12, 13]. In 2003, Pilloud and Dehlinger fabricated a zirconium nitride film through magnetron sputtering using an Alcatel SCM650 sputtering system. They investigated the effect of changing substrate bias, substrate temperature, and nitrogen gas flow on structural and mechanical properties [14]. In 2003, Hu and Li deposited zirconium nitride on the glass substrate by a magnetron sputtering with different nitrogen gas flows in an argon and nitrogen gas mixture. They showed that if the flow of nitrogen ( $F(N_2)$ ) is between 5 and 12 %, the film with NaCl structure (fcc) with the preferred direction is formed.  $ZrN_x$  structure does not change with increasing nitrogen flow from 12 to 24 %, and  $ZrN(111)$  peak is the preferred direction. When  $F(N_2)$  is more than 24 %, no more peak is observed, which means that  $ZrN_x$  films are formed in an amorphous form [15]. Han, Lee, and colleagues subjected zirconium to nitrogen ion implantation. By examining the wear test results, they found that with the process of nitrogen implantation and formation of zirconium nitride, the wear of zirconium decreases with the increase of the ion dose, and the wear also decreases [16].

The first step of this research involved depositing thin films of zirconium onto 304 steel substrates using an ion-sputtering device. Then a thin zirconium nitride film was made using an ion implantation accelerator with a constant ion dose at different energies. In the following, its structural properties, corrosion behavior, and SEM analysis after the corrosion test have been investigated as a function of implantation energy. The deposition techniques used are chosen due to their

ability to precisely control the thickness of the coating and produce a uniformly coated surface with superior adhesion.

## 2. Experimental

In this study, Zirconium nitride thin films with a thickness of 100 nm were deposited on AISI 304 stainless steel substrates by ion beam sputtering (IBS) at room temperature. Table 1 [17] provides information on the chemical composition and element abundance of the stainless steel alloy employed in the study. Ion beam sputtering is a highly effective coating method that uses ion beams to apply materials onto a substrate's surface. The schematic diagram of the IBS for the deposition of ZrN films is shown in Figure 1. This study accelerated Ar ions toward a Zr target at a fixed energy of 2.2 keV and a 25 mA/cm<sup>2</sup> current throughout the experimental process. The substrate temperature during deposition was consistently maintained at 400 °C. For a more detailed overview of the deposition conditions, please refer to Table 2. The purity of the zirconium target used in the experiment was 99.98 %. The deposition process was carried out in an advanced (E19 A3 Edwards, England) coating plant, which maintained a base pressure of  $2 \times 10^{-5}$  mbar. A quartz crystal deposition rate controller (Sigma Instruments, SQM-160, USA) was positioned close to the substrates to measure the deposition rate precisely.

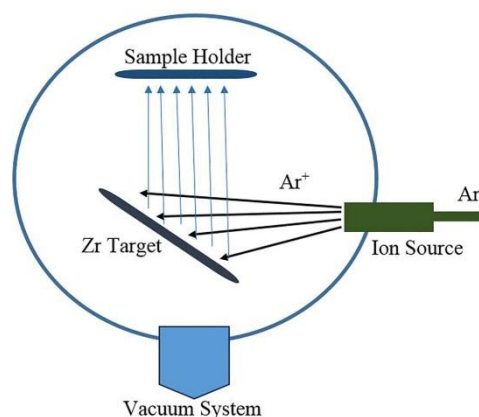
To safeguard against scratching and oxidation, the production factory shielded the stainless steel substrates with a protective polyethylene sheet. The sheet was removed by soaking the substrates in ethanol, which were cut to a size of  $20 \times 20 \times 1$  mm. Before deposition, all substrates underwent a thorough ultrasonic cleaning process in heated acetone and ethanol. Nitrogen ion implantation of the samples was done at a temperature of 400 °C, a dose of  $5 \times 10^{17}$  N<sup>+</sup>/cm<sup>2</sup>, and four different energies of 10, 20, 40, and 80 keV.

**Table 1:** Chemical composition and abundances (%) of different elements in 304 stainless steels [17].

SS Type	Fe	Cr	Ni	Mn	Si	C	P	S
SS(304)	66-71	18-20	8-10.5	2	1	0.08	0.045	0.03

**Table 2:** The deposition conditions for zirconium nitride thin films by ion beam sputtering.

Deposition parameters specifications	
Target	Zirconium
Sputtering gas	Argon
Base pressure (mbar)	$2 \times 10^{-5}$
Working Pressure (mbar)	$4 \times 10^{-3}$
Substrate temperature ( $^{\circ}\text{C}$ )	400
Electron beam current (mA)	25
Acceleration voltage (kV)	2.2
Deposition time (min)	40
$\text{N}^+$ dose ( $\text{N}^+/\text{cm}^2$ )	$5 \times 10^{17}$
Implantation energy (keV)	10, 20, 40, 80

**Figure 1:** Schematic diagram of the Ion Beam Sputtering system.

The crystallographic structure of the thin films was analyzed using a STOE model STADI MP Diffractometer from Germany, which employed  $\text{CuK}\alpha$  radiation and used a step size of  $0.01^{\circ}$  with a count time of 1.0 s per step. The surface physical morphology and nanostructure were characterized using a scanning electron microscope (SEM: LEO 440i, England). The hardness of the samples was determined by a Vickers microhardness tester (Leitz Hardness Tester). A weight of 25 g was used for applying a force equal to  $25.254 \times 10^{-4}$  N on the surface. The electrochemical behavior of the samples was assessed using the potentiodynamic polarization method and device (IVIUM-Compact-State 20250 model). A specially designed holder was used to ensure precise measurements, exposing only a surface area of  $1 \pm 0.05 \text{ cm}^2$  to the corrosive environment. The test medium consisted of a 0.6 M NaCl solution, with Ag/AgCl and platinum electrodes as a reference and auxiliary electrodes, respectively.

The samples produced were utilized as working electrodes in the electrochemical cell. All potentials used were expressed relative to  $V_{\text{OCP}}$ , with the starting potential set at -400 mV relative to  $V_{\text{OCP}}$ .

### 3. Results and Discussion

#### 3.1. Crystal structure analysis

The XRD patterns of the untreated and coated samples with different implantation energies are shown in Figure 2. As expected, three iron peaks related to 304 steel are observed as substrate peaks in the spectrum of samples. Zirconium nitride peaks are observed in the sample produced by the implantation process with 10 keV energy. As it is known,  $\text{ZrN}(111)$  peak has the highest intensity. Therefore, the preferred direction in the film belongs to this peak. In this sample, zirconium nitride can also be seen on peaks of (200), (220), (222), and (311).

Increasing the implantation energy to 20 keV, increases the intensity of the peak belonging to ZrN(111). This increase is also observed in other zirconium nitride peaks. Also, increasing the implantation energy to 40 keV, increases the intensity of the peak in the preferred direction (111). The intensity of the peaks related to the (200), (220), (311), and (222) directions has been increased compared to the previous sample. By increasing the implantation energy to 80 keV, the intensity of the peak belonging to the (111) peak of zirconium nitride has decreased significantly. For the other peaks, the intensity decrease is visible. In other words, increasing the implantation energy to 80 keV has resulted in the disruption of the arrangement of the crystal plates, leading to a reduction in the level of crystallization.

By comparing the peaks, it is concluded that by increasing the implantation energy up to 40 keV, the intensity of the zirconium nitride peak or the degree of crystallization has increased, reaching its maximum value for 40 keV energy. However, at the maximum energy of 80 keV, the intensity of the zirconium nitride peaks decreases and reaches its lowest value, and the degree of crystallization decreases.

By using Scherer's law and the diffraction pattern of different samples, it is possible to calculate the crystal size (Eq. 1):

$$d = \frac{k\lambda}{D \cos\theta} \quad (1)$$

Where d: the crystal size,  $\lambda$ : wavelength, D: Full width at half maximum (FWHM),  $\theta$ : Bragg angle, k: constant value 0.9 [10].

The crystal size of the samples for different amounts of implantation energy is calculated and given in Table 3. Increasing the implantation energy up to 40 keV makes the crystal size larger. The crystal size has decreased for the sample produced at the highest implantation energy, equivalent to 80 keV.

### 3.2. Hardness measurement

The samples produced at different implantation energies were studied to check the mechanical properties, including hardness. Table 3 exhibits implantation energy's influence on the produced samples' hardness. The hardness of the samples deposited on 304SS was measured using a Vickers microhardness tester and calculated using the following equation (Eq. 2):

$$H_v = 2 \cos 22^\circ \frac{F}{l_v^2} = 1.854 \frac{F}{l_v^2} \text{ kg/mm}^2 \quad (2)$$

Where  $l_v$  is the diameter of the rhombus or pyramid, and F is the weight mass [1].

The measured values for the samples can be used as long as the indentation rate is about one-tenth or less than the thickness of the film so that the hardness of the sample does not affect the hardness of the combination of the film and the substrate.

Considering the constant conditions of the process in all the samples, a weight of 25 grams was used. As seen in Table 3, the hardness increases and then decreases by increasing implantation energy. By increasing the implantation energy up to 40 keV, initially, the hardness increased, and for the maximum implantation energy of 80 keV, the hardness of the sample decreased.

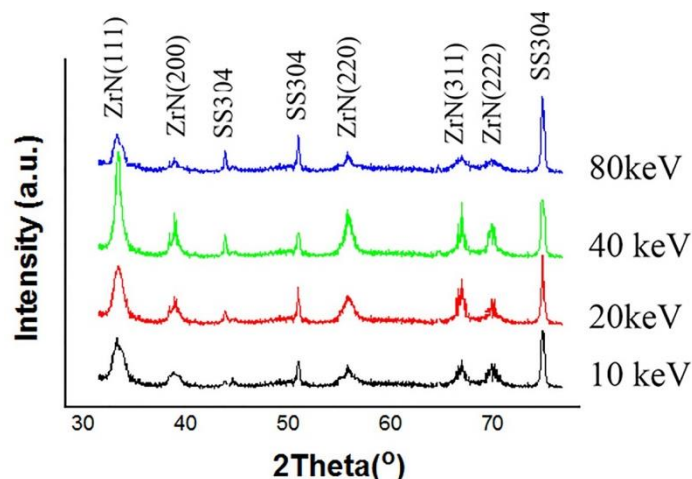


Figure 2: The crystallographic pattern of different samples produced at different implantation energies.

**Table3:** Calculated crystal size for (111) preferred direction and hardness of different samples.

Implantation energy (keV)	10	20	40	80
Crystal size (nm)	28	54	76	22
Film hardness	362	454	561	417

**Table 4:** Corrosion parameters of samples produced on 304SS substrates.

Sample	Energy (keV)	Corrosion current density ( $\mu\text{A cm}^{-2}$ )	Corrosion potential (V vs. SCE)
304 SS	---	17.7828	-0.363
Implanted samples	1	10	0.4897
	2	20	0.1862
	3	40	0.0194
	4	80	4.3651

### 3.3. Potentiodynamic polarization

Potentiodynamic curves of the bare 304 stainless steel substrates and those implanted at various energies of 10, 20, 40, and 80 keV are shown in Figure 3. The polarization plot shows that the deposition of ZrN on the stainless steel substrate improves its corrosion resistance. Figure 4 shows that the polarization plot of treated 304SS samples has shifted towards lower corrosion current density and higher corrosion potential, which indicates that corrosion protection has improved for these samples. As can be seen in Table 4, for the 304SS sample that has been implanted in 40 keV, the optimal value of corrosion current density and corrosion potential were obtained as  $0.0194 \mu\text{A/cm}^2$  and  $0.020 \text{ V vs SCE}$ , respectively; in contrast, these values for bare 304SS substrate were obtained  $17.7828 \mu\text{A/cm}^2$  and  $-0.363 \text{ V vs SCE}$ .

For optimal measured hardness and maximum corrosion resistance, a critical value of 40 keV is observed. The XRD results also showed that the intensity of ZrN(111) was highest at this implantation energy. Therefore, it can also be concluded that the volume of zirconium nitride formed on this sample is more significant than that produced at lower and higher energies. Therefore, all of the above discussions point to correlations between the results reported in this study.

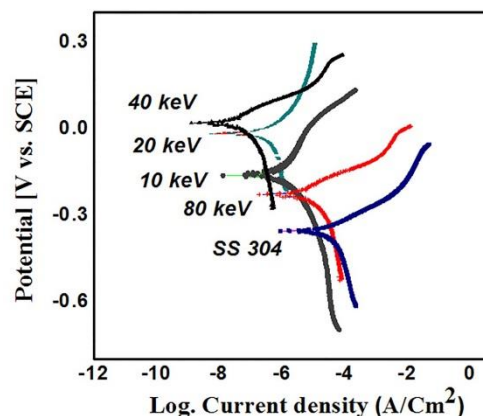


**Figure 3:** Potentiodynamic polarization curves for 304SS and Zr/304SS samples implanted at different energies.

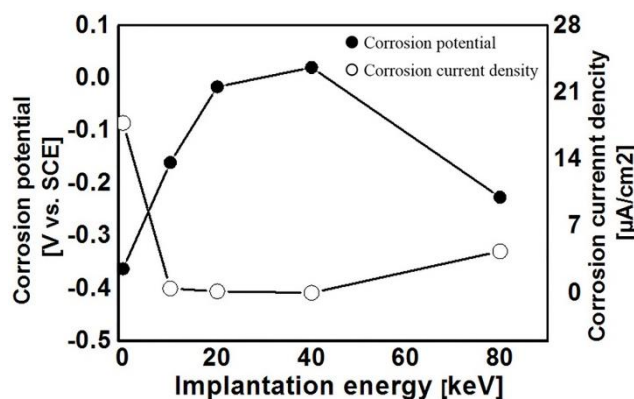


**Figure 4:** Variations of corrosion potential and corrosion current density as a function of implantation energy for 304SS and Zr/304SS samples implanted at different energies.

### 3.4. SEM Analysis

Figure 5 presents the surface morphologies of the implanted samples at different implantation energy and the untreated 304 stainless steel substrate after undergoing corrosion tests. The uncoated substrate (Figure 5a) displays obvious signs of corrosion attack and dissolution distributed across the sample's surface. However, the SEM images of implanted samples show different morphologies with varying types and sizes of corrosion effects, such as pits, cracks, peel-offs, and dissolutions. From Figure 5, it is evident that the sample implanted at 40 keV (Figure 5d) exhibits the least amount of corrosion effects mentioned above, and it has also produced the best results for the potentiodynamic test. On the surface of the samples

implanted at 10, 20, and 80 keV, pits and peel-offs of the zirconium nitride layer or deeper attacks of the corroding medium into the SS substrates (Figure 5e) can be distinguished in comparison small pits or imperfections have caused an almost uniform distribution of corrosion on the surface of the sample implanted at 20 keV (Figure 5c). These features can be likened to bubbles on the film surface that may also be expected during the corrosion or reaction.

Upon implanting the sample at the highest energy level of 80 keV, the resulting SEM image reveals a significant deterioration in the surface of the zirconium nitride coating such that the corrosive solution can penetrate the steel substrate and ultimately causes the complete removal of the layer.

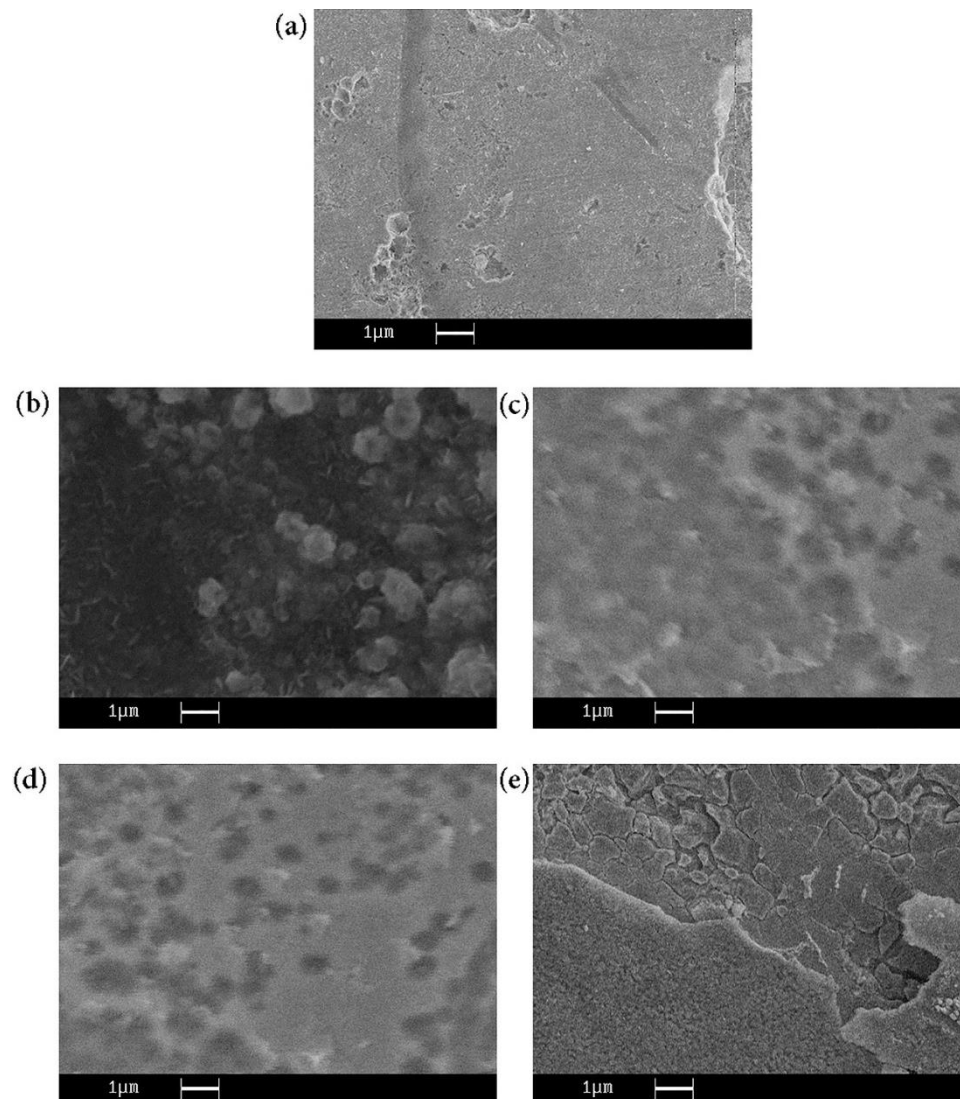


**Figure 5:** SEM images of different samples produced at different implantation energies: (a) 304 SS, (b) 10 keV, (c) 20 keV, (d) 40 keV and (e) 80 keV.

#### 4. Conclusion

Zirconium nitride thin films were deposited on 304 stainless steel substrates at 400 °C and then implanted at different energies. The XRD pattern of ZrN/SS samples shows the formation of the ZrN crystal phase with the preferred growth direction (111). The peak intensity corresponding to this direction increases with the implantation energy up to 40 keV. Increasing the implantation energy to 80 keV has decreased (111) peak intensity. With the increase of energy up to the

optimal value of 40 keV, the hardness of the samples had an upward trend and then decreased. The maximum measured hardness value is equal to 561 Hv. The sample implanted in the energy of 40 keV with a corrosion current density of 0.0194  $\mu\text{A cm}^{-2}$  and a corrosion potential of 0.02 V has optimal results for corrosion resistance in the test environment. The optimal sample also showed the most intact surface after the corrosion test in SEM images.

#### 5. References

1. M. Ohring, materials science of thin films, Academic press, New York, 1991.
2. L. Eckertova, Physics of Thin Films, Plenum Press, New York, 1990.
3. C.-H Ma, J.-H. Huang, H. Chen, A study of preferred orientation of vanadium nitride and zirconium nitride coatings on silicon prepared by Ion beam assisted deposition, *Surf. Coat.*, 133-134(2000), 289-294.
4. A. R. Grayeli Korpi, Kh. M. Bahmanpour, Effect of nitriding temperature on the nanostructure and corrosion properties of nickel coated 304 stainless steel, *Prog. Color Colorants Coat.*, 10(2017), 85-92.
5. K. I. Aly, A. Mahdy, M. A. Hegazy, N. S. Al-Muaike, S.W. Kuo, M. G. Mohamed, Corrosion resistance of mild steel coated with Phthalimide-functionalized polybenzoxazines, *Coatings*, 10(2020), 1114.
6. M. G. Mohamed, S.W. Kuo, A. Mahdy, I.M. Ghayd, K. I. Aly, Bisbenzylidene cyclopentanone and cyclohexanone-functionalized polybenzoxazine nanocomposites: Synthesis, characterization, and use for corrosion protection on mild steel, *Mater. Today Commun.*, 25(2020), 101418.
7. K. I. Aly, M. G. Mohamed, O. Younis, M. H. Mahross, M. Abdel-Hakim, M. M. Sayed, Salicylaldehyde azine-functionalized polybenzoxazine: Synthesis, characterization, and its nanocomposites as coatings for inhibiting the mild steel corrosion, *Prog. Org. Coat.*, 138(2020), 105385.
8. M. G. Mohamed, A. Mahdy, R. J. Obaid, M. A. Hegazy, S.W. Kuo, K. I. Aly, Synthesis and characterization of polybenzoxazine/clay hybrid nanocomposites for UV light shielding and anti-corrosion coatings on mild steel, *J. Polym. Res.*, 28(2021), 297.
9. J. A. Garcia, A. Guette, A. Medrano, C. Labrugere, M. Rico, M. Lahaye, R. Sanchez, A. Martinez, R. J. Rodriguez, Nitrogen Ion implantation on group IVb metals: chemical, mechanical and tribological, *Vacuum*, 64(2002), 343-351.
10. R. J. Rodriguez, J. A. Garcia, A. Medrano, M. Rico, R. Sanchez, R. Martinez, C. Labrugere, M. Lahaye, A. Guette, Tribological behaviour of hard coatings deposited by arc-evaporation PVD, *Vacuum*, 67(2002), 559-566.
11. J.H. Huang, C.Y. Hsu, S.S. Chen, G.P. Yu, Effect of substrate bias on the structure and properties of Ion-plated ZrN on Si and stainless steel substrates, *Mater. Chem. Phys.*, 77(2003), 14-21.
12. W. J. Chou, G. P. Yu, J. H. Huang, Bias effect of Ion-plated Zirconium nitride film on Si (100), *Thin Solid Films*, 405(2002), 162-169.
13. A. R. Grayeli Korpi, Kh. M. Bahmanpour, Influence of nitrogen Ion implantation on the structure and corrosion resistance of stainless steel substrates coated with Ni nanolayer, *Prog. Color Colorants Coat.*, 9(2016), 77-83.
14. D. Pilloud, A. S. Dehlinger, J. F. Pierson, A. Roman, I. Pichon, Reactively sputtered zirconium nitride coating: structural, mechanical, optical and electrical characteristics, *Surf. Coat.*, 174-175 (2003), 338-344.
15. L. Hu, D. Li, G. Fang, Influence of  $\text{N}_2(\text{N}_2+\text{Ar})$  flow ratio and substrate temperature on the properties of Zirconium nitride films prepared by reactive DC magnetron sputtering, *Appl. Surf. Sci.*, 220(2003), 367-371.
16. J.G. Han, J.S. Lee, B.H. Choi, W. Kim, G. Tang, Wear and fretting wear behaviour of ion-implanted zircaloy-4, *Surf. Coat.*, 83(1996), 307-312.
17. J.R. Davis, ASM Specialty Handbook: Stainless Steels (Materials OH: ASM International, 1994), 22.

How to cite this article:

M. Karimi, A.R. Grayeli, Analysis of Nitrogen Ion Implantation on Corrosion Inhabitation of Zirconium Nitride Coated 304 Stainless Steel and Correlation with Nano-structure and Surface Hardness. *Prog. Color Colorants Coat.*, 16 (2023), 409-415.

